Random matrix ensemble for the covariance matrix of Ornstein-Uhlenbeck processes with heterogeneous temperatures

Leonardo S. Ferreira and Fernando L. Metz
Physics Institute, Federal University of Rio Grande do Sul, 91501-970 Porto Alegre, Brazil

Paolo Barucca
Department of Computer Science, University College London, WC1E 6BT London, United Kingdom

We introduce a random matrix model for the stationary covariance of multivariate Ornstein-Uhlenbeck processes with heterogeneous temperatures, where the covariance is constrained by the Sylvester-Lyapunov equation. Using the replica method, we compute the spectral density of the equal-time covariance matrix characterizing the stationary states, demonstrating that this model undergoes a transition between stable and unstable states. In the stable regime, the spectral density has a finite and positive support, whereas negative eigenvalues emerge in the unstable regime. We determine the critical line separating these regimes and show that the spectral density exhibits a power-law tail at marginal stability, with an exponent independent of the temperature distribution. Additionally, we compute the spectral density of the lagged covariance matrix characterizing the stationary states of linear transformations of the original dynamical variables. Our random-matrix model is potentially interesting to understand the spectral properties of empirical correlation matrices appearing in the study of complex systems.

I. INTRODUCTION

The history and success of random matrix theory demonstrate that diverse data sets, regardless of their origin, can display universal patterns in their spectral decomposition [1]. Random matrix theory has been applied to various fields, including quantum physics [2, 3], climate time series [4], functional MRI [5] and financial data [6, 7]. The underlying interactions in large complex systems – such as neural networks, ecosystems, and stock markets [8–10] – are typically inferred from the empirical covariances among the system's states. Random matrix theory plays a pivotal role in the problem of estimating the covariance matrix from noisy data obtained from high-dimensional dynamical systems [11–13].

The dynamical variables describing complex systems evolve in time according to nonlinear differential equations [14]. The stability of fixed-points is crucial to understand the behavior of these systems [15, 16]. For example, a stable ecosystem is often associated with a stable fixed-point [17, 18], where species abundances exhibit small fluctuations around their average values [19, 20]. However, as model parameters change, stable fixed-points can become unstable [18, 21, 22], leading to a variety of dynamical behaviors, including chaos and periodic oscillations [14, 20, 23, 24]. A popular conjecture suggests that complex systems have adapted to operate at marginal stability [25–28], i.e., near the critical point of the stability transition. In this situation, large fluctuations of the dynamical variables result in power-law distributions of various quantities. For instance, economic models show power-law fluctuations in prices and firm sizes [27], models of ecosystems display a power-law singularity in their power-spectrum [19], and neuronal activity distributions exhibit power-law tails [26]. Despite the importance of the covariance matrix as an experimentally accessible quantity, a systematic analysis of how its spectral properties behave across the stability transition has remained elusive.

Random matrix theory provides benchmark models for empirical covariance matrices [7], allowing to distinguish between eigenvalues representing pure randomness from those reflecting genuine correlations within the system [12, 29, 30]. Random-matrix models of covariance matrices rely on *ad hoc* assumptions for the statistics of the matrix entries [7, 30–35]. The most prominent example is the so-called Wishart ensemble [36], where the covariance matrix is constructed by multiplying a pair of rectangular matrices with Gaussian-distributed entries. The main advantage of the Wishart ensemble is that many spectral properties can be analytically computed [12, 37–40]. However, a significant drawback is that this model does not account for the interactions within the system, making it unsuitable for studying how the stability transition affects the spectral properties of the covariance matrix.

In general, there is no direct relationship between the covariance matrix and the interactions in complex systems due to the nonlinearity of the dynamics. However, if the dynamical equations can be linearized near the stability transition [41], the dynamics simplify to a multivariate Ornstein-Uhlenbeck process (MVOU) [42, 43]. In this linear regime, the stationary covariance matrix satisfies the Sylvester-Lyapunov equation [44, 45], which depends solely on the diffusion and interaction matrices defining the process. This framework opens the possibility of introducing covariance matrix ensembles that explicitly account for interactions, potentially improving our understanding of stability transitions through the analysis of the covariance spectrum.

Building on previous work [46], we introduce an ensemble of covariance matrices derived from the stationary states of reversible MVOU processes, where each

random matrix instance is a solution of the Sylvester-Lyapunov equation. Thus, this ensemble incorporates the constraints imposed by the Sylvester-Lyapunov equation, resulting in a model where the covariance matrix is determined by the interaction and diffusion matrices. By considering fully-connected Gaussian interactions and a diagonal diffusion matrix, with elements representing the local temperatures of the dynamical variables, we study how the temperature distribution influences the spectrum of the covariance across the stability transition.

Using the replica method of disordered systems [47], we derive analytic results for the spectral densities of both the equal-time covariance matrix and the lagged covariance matrix, with the latter resulting from a generic linear transformation of the original dynamical process. These results enable a systematic investigation of how the stability transition impacts the spectral density. In the stable regime, the eigenvalues are positive and the spectral density $\rho_S(\lambda)$ of the equal-time covariance $\boldsymbol{S}$ is supported on a finite interval, while the unstable phase is marked by the appearance of negative eigenvalues. At marginal stability, all eigenvalues remain positive and $\rho_S(\lambda)$ exhibits a power-law tail $\rho_S(\lambda) \propto \lambda^{-5/2}$, with an exponent independent of the temperature distribution. This finding suggests that the power-law decay of $\rho_S(\lambda)$ is an universal property of complex systems at marginal stability.

The paper is organized as follows. In section II, we introduce reversible MVOU processes and derive general solutions for the covariance and lagged covariance matrices as functions of coupling strengths and temperatures. Section III defines the specific ensembles of covariance matrices. In Section IV, we present analytic results for the spectral densities of the covariance matrices for arbitrary temperature distributions. Section V provides numerical results for specific temperature distributions, confirming our theoretical predictions and illustrating the behavior of the spectral density of the equal-time covariance across the stability transition. Finally, the last section summarizes our results and indicates possible directions of future research. The paper includes an appendix detailing the replica calculations of the spectral densities.

II. MULTIVARIATE ORNSTEIN-UHLENBECK PROCESSES

We consider N dynamical variables $X_1(t), \dots, X_N(t)$ that may represent the abundances of different species in an ecosystem, the neuronal activities in the brain, or the stock prices of a financial system. The degrees of freedom $\boldsymbol{X}(t) = (X_1(t), \dots, X_N(t))^T$ evolve in time according to a multivariate Ornstein-Uhlenbeck process (MVOU), which is represented by the coupled system of stochastic differential equations

$$d\boldsymbol{X} = -\boldsymbol{A}\boldsymbol{X}dt + \boldsymbol{\eta}\sqrt{dt}, \tag{1}$$

where $\eta_i(t)$ is a Gaussian noise with zero mean and covariance

$$\langle \eta_i(t)\eta_j(t')\rangle_\eta = 2D_{ij}\delta(t-t'). \tag{2}$$

The element A_{ij} of matrix $\boldsymbol{A}$ quantifies the influence of $X_j(t)$ on $X_i(t)$, while the element D_{ij} of the symmetric positive-definite matrix $\boldsymbol{D}$ controls the covariance between $\eta_i(t)$ and $\eta_j(t)$. The coupling matrix $\boldsymbol{A}$ and the diffusion matrix $\boldsymbol{D}$ completely specify the model. The Gaussian noise variables $\eta_1(t), \dots, \eta_N(t)$ account for environmental random perturbations.

The central object of our interest is the two-time covariance matrix $\boldsymbol{S}(s,t)$ of the dynamical variables. The elements of this $N \times N$ matrix are given by

$$S_{ij}(s,t) = \langle X_i(s)X_j(t)\rangle_\eta, \tag{3}$$

where $\langle \dots \rangle_\eta$ denotes the ensemble average over the Gaussian noise. Equation (1) converges to a stable stationary solution provided the real parts of all eigenvalues of $\boldsymbol{A}$ are positive [42]. In this case, the joint distribution of $X_1(t), \dots, X_N(t)$ evolves to a multivariate Gaussian distribution characterized by the equal-time covariance matrix $\boldsymbol{S}$, whose elements read

$$S_{ij} = \lim_{t\to\infty} \langle X_i(t)X_j(t)\rangle_\eta. \tag{4}$$

In addition, one can show that, in the stationary regime, the matrices $\boldsymbol{S}$, $\boldsymbol{A}$ and $\boldsymbol{D}$ fulfill the relation [44]

$$\boldsymbol{A}\boldsymbol{S} + \boldsymbol{S}\boldsymbol{A}^T = 2\boldsymbol{D}, \tag{5}$$

known as the Sylvester-Lyapunov equation. One of the aims of our work is to introduce a random-matrix ensemble for the covariance matrix $\boldsymbol{S}$ which incorporates the above constraint.

Here we focus on MVOU processes that satisfy the Onsager reversibility conditions [44], expressed in matrix form as follows

$$\boldsymbol{A}\boldsymbol{D} = \boldsymbol{D}\boldsymbol{A}^T. \tag{6}$$

The reversibility constraint imposes a strong interdependence between the elements of the coupling and diffusion matrices. For systems that fulfill Eq. (6), the Sylvester-Lyapunov equation admits the general solution

$$\boldsymbol{S} = \boldsymbol{A}^{-1}\boldsymbol{D}. \tag{7}$$

Thus, in order to put forward a random-matrix ensemble for $\boldsymbol{S}$, we just need to sample $\boldsymbol{A}$ and $\boldsymbol{D}$ subject to Eq. (6), since the constraint imposed by the Sylvester-Lyapunov equation is automatically fulfilled by Eq. (7). We point out that $\boldsymbol{S}$ and $\boldsymbol{D}$ are symmetric matrices, while $\boldsymbol{A}$ is not necessarily symmetric.

In reversible systems, we can also extract information about the lagged covariance in the stationary regime. Let $R_{ij}(t,s)$ be the two-time response function

$$R_{ij}(t,s) = \frac{\delta\langle X_i(t)\rangle_\eta}{\delta h_j(s)}, \tag{8}$$

where $h_j(s)$ is a time-dependent external field that linearly couples to $X_j(s)$ in Eq. (1). In the stationary regime, both $R_{ij}(t,s)$ and $S_{ij}(t,s)$ are invariant under time-translation, i.e., $R_{ij}(t,s) = R_{ij}(\tau)$ and $S_{ij}(t,s) = S_{ij}(\tau)$, with $\tau = t - s \geq 0$. The quantity $S_{ij}(\tau)$ is the lagged covariance between $X_i(t)$ and $X_j(t+\tau)$ in the stationary regime. In terms of the $N \times N$ matrices $\boldsymbol{R}(\tau)$ and $\boldsymbol{S}(\tau)$, one can show that [44]

$$\boldsymbol{R}(\tau) = \exp\left(-\tau \boldsymbol{A}\right), \tag{9}$$

and

$$\boldsymbol{S}(\tau) = \exp\left(-\tau \boldsymbol{A}\right)\boldsymbol{S}. \tag{10}$$

For reversible MVOU processes, $\boldsymbol{S}(\tau)$ is a symmetric matrix. Although Eq. (10) provides an interesting expression for the lagged covariance $\boldsymbol{S}(\tau)$, $\boldsymbol{S}$ and $\boldsymbol{A}$ do not share the same eigenvectors. Thus, even if we know the eigenvalues of $\boldsymbol{S}$ and $\boldsymbol{A}$, Eq. (10) does not give access to the spectrum of $\boldsymbol{S}(\tau)$.

Since MVOU processes are described by linear equations, one can make a change of dynamical variables and derive a more useful expression for the lagged covariance matrix in the transformed system. Let $\boldsymbol{X}' = \boldsymbol{B}^{-1}\boldsymbol{X}$ be the new vector of dynamical variables, with $\boldsymbol{B}$ an arbitrary matrix. Multiplying Eq. (1) on the left by $\boldsymbol{B}^{-1}$ and using the decomposition $\boldsymbol{D} = \boldsymbol{B}\boldsymbol{B}^T$ of positive-definite matrices, one can show that $\boldsymbol{X}'$ fulfills

$$d\boldsymbol{X}' = -\boldsymbol{A}'\boldsymbol{X}'dt + \boldsymbol{\eta}'\sqrt{dt}, \tag{11}$$

where the new coupling matrix $\boldsymbol{A}'$ and the covariance matrix $\boldsymbol{D}'$ associated to $\boldsymbol{\eta}'$ are, respectively, given by $\boldsymbol{A}' = \boldsymbol{B}^{-1}\boldsymbol{A}\boldsymbol{B}$ and $\boldsymbol{D}' = \boldsymbol{I}$, with $\boldsymbol{I}$ denoting the identity matrix. From the reversibility condition, Eq. (6), we conclude that $\boldsymbol{A}'$ is symmetric. In addition, by inverting the relation between $\boldsymbol{A}'$ and $\boldsymbol{A}$, it is straightforward to verify that

$$\boldsymbol{A} = \boldsymbol{D}\boldsymbol{J}, \tag{12}$$

where $\boldsymbol{J} = (\boldsymbol{B}^T)^{-1}\boldsymbol{A}'\boldsymbol{B}^{-1}$ is a symmetric matrix. Hence, the coupling matrix $\boldsymbol{A}$ of reversible MVOU processes can be always decomposed as a product between the noise covariance $\boldsymbol{D}$ and a symmetric matrix $\boldsymbol{J}$. The reversibility condition is automatically fulfilled by the matrix decomposition of Eq. (12).

In the transformed system, since the stationary state is characterized by the covariance $\boldsymbol{S}' = \boldsymbol{A}'^{-1}$, both the response matrix $\boldsymbol{R}'(\tau)$ and the lagged covariance matrix $\boldsymbol{S}'(\tau)$ read

$$\begin{aligned} \boldsymbol{R}'(\tau) &= \exp(-\tau\boldsymbol{A}'), \\ \boldsymbol{S}'(\tau) &= \exp(-\tau\boldsymbol{A}')\boldsymbol{A}'^{-1}. \end{aligned} \tag{13}$$

Therefore, the equal-time covariance $\boldsymbol{S}'$, the lagged covariance $\boldsymbol{S}'(\tau)$ and the response $\boldsymbol{R}'(\tau)$ share the eigenvectors of the transformed coupling matrix $\boldsymbol{A}'$. Once we know the eigenvalues of $\boldsymbol{A}'$, it is straightforward to determine, for instance, the eigenvalues of the lagged covariance $\boldsymbol{S}'(\tau)$ as a function of time τ.

Finally, let us understand how $\boldsymbol{S}'(\tau)$ and $\boldsymbol{S}(\tau)$ are related. By using the transformation rule $\boldsymbol{A}' = \boldsymbol{B}^{-1}\boldsymbol{A}\boldsymbol{B}$, Eq. (13) can be written as

$$\boldsymbol{S}'(\tau) = \sum_{n=0}^{\infty} \frac{(-\tau)^n}{n!}\boldsymbol{B}^{-1}\boldsymbol{A}^n\boldsymbol{A}^{-1}\boldsymbol{B}. \tag{14}$$

By substituting $\boldsymbol{B} = \boldsymbol{D}(\boldsymbol{B}^T)^{-1}$ in the above equation and using Eq. (7), we obtain

$$\boldsymbol{S}(\tau) = \boldsymbol{B}\boldsymbol{S}'(\tau)\boldsymbol{B}^T. \tag{15}$$

Clearly, the spectral density of $\boldsymbol{S}'(\tau)$ does not give direct access to the spectral density of $\boldsymbol{S}(\tau)$, because in general $\boldsymbol{B}$ and $\boldsymbol{S}'(\tau)$ do not share the same eigenvectors. In spite of that, from the spectra of $\boldsymbol{B}$ and $\boldsymbol{S}'(\tau)$, we can derive bounds on the eigenvalues of $\boldsymbol{S}(\tau)$ [48, 49]. In particular, in appendix B we obtain bounds for the smallest and largest eigenvalues of $\boldsymbol{S}(\tau)$ when $\boldsymbol{D}$ is a diagonal matrix.

III. THE RANDOM-MATRIX ENSEMBLE

We are interested in the spectral properties of the covariance $\boldsymbol{S}$ and the lagged covariance $\boldsymbol{S}'(\tau)$ that characterize reversible MVOU processes. We will follow the random-matrix prescription and assume that the coupling strengths are drawn from an ensemble of random matrices subject to the constraints dictated by Eqs. (6) and (7).

In the previous section, we have shown that $\boldsymbol{A}$ can be decomposed as $\boldsymbol{A} = \boldsymbol{D}\boldsymbol{J}$, where $\boldsymbol{J}$ is a symmetric matrix that, in principle, might depend on $\boldsymbol{D}$. The choice of $\boldsymbol{J}$ thus defines the random-matrix model for the interaction matrix $\boldsymbol{A}$. Here, we consider that $\boldsymbol{J}$ has the generic form

$$\boldsymbol{J} = \mu\boldsymbol{D}^{-1} + g(\boldsymbol{D})\boldsymbol{K}g(\boldsymbol{D}), \tag{16}$$

in which $\mu > 0$, $\boldsymbol{K}$ is a symmetric matrix with real-valued entries, and $g(\boldsymbol{D})$ is a matrix function of the diagonal covariance $\boldsymbol{D}$, with elements

$$D_{ij} = T_i\delta_{ij}, \tag{17}$$

where T_i is the local temperature of the dynamical variable $X_i(t)$. The first term $\mu\boldsymbol{D}^{-1}$ in Eq. (16) ensures that $\boldsymbol{A}$ is positive-definite for sufficiently large $\mu > 0$, which allows us to control the stability of the dynamics by varying μ. The second term in Eq. (16) is responsible for the pairwise interactions among the dynamical variables. With the purpose of explicitly incorporating the effect of heterogeneous temperatures in $\boldsymbol{A}$, this term is given by a symmetric matrix $\boldsymbol{K}$ deformed by a generic function $g(\boldsymbol{D})$ of the diffusion matrix. The interaction matrix $\boldsymbol{A}$ and its transformed version $\boldsymbol{A}'$ are thus given by

$$\boldsymbol{A} = \mu\boldsymbol{I} + \boldsymbol{D}g(\boldsymbol{D})\boldsymbol{K}g(\boldsymbol{D}) \tag{18}$$

and

$$\boldsymbol{A}' = \mu \boldsymbol{I} + \boldsymbol{D}^{1/2} g(\boldsymbol{D}) \boldsymbol{K} g(\boldsymbol{D}) \boldsymbol{D}^{1/2}. \tag{19}$$

The above equations determine the equal-time covariance and the lagged covariance via Eqs. (7) and (13). By tuning $\mu > 0$, we ensure that MVOU processes governed by Eqs. (1) and (11) converge to stationary Gaussian distributions.

We are now ready to formally define the reversible random-matrix ensemble that we study in the following sections. The diagonal elements of $\boldsymbol{K}$ are zero, while the off-diagonal elements $K_{ij} = K_{ji}$ $(i \neq j)$ are independent and identically distributed random variables drawn from a Gaussian distribution with mean zero and variance $1/N$. In addition, the local temperatures $T_1, \ldots, T_N$ are independent and identically distributed variables sampled from $p(T)$. The coupling matrix $\boldsymbol{A}$ can be seen as a deformed Wigner matrix, in which a Gaussian random matrix is multiplied on both sides by a generic function of the diagonal diffusion matrix $\boldsymbol{D}$ and then added to a diagonal matrix.

Our primary aim is to compute the spectral density of $\boldsymbol{S}$. Substituting Eq. (18) in Eq. (7), we obtain the covariance

$$\boldsymbol{S} = (\mu \boldsymbol{I} + \boldsymbol{D} g(\boldsymbol{D}) \boldsymbol{K} g(\boldsymbol{D}))^{-1} \boldsymbol{D}, \tag{20}$$

and the so-called precision matrix

$$\boldsymbol{S}^{-1} = \mu \boldsymbol{D}^{-1} + g(\boldsymbol{D}) \boldsymbol{K} g(\boldsymbol{D}). \tag{21}$$

The spectral density of $\boldsymbol{S}$ is obtained from the spectral density of $\boldsymbol{S}^{-1}$ by a simple change of variables. As we show below, the spectral density of $\boldsymbol{S}$ can be analytically computed in the limit $N \to \infty$, which is an appealing feature of the random-matrix model introduced by Eq. (16).

IV. SPECTRAL DENSITY OF THE COVARIANCES MATRICES

In this section, we present analytic results for the spectral densities of both $\boldsymbol{S}$ and $\boldsymbol{S}'(\tau)$ in the limit $N \to \infty$. Before discussing our main results, we introduce some useful notation. Let $\{\lambda_i(\boldsymbol{X})\}_{i=1,\ldots,N}$ denote the (real) eigenvalues of an $N \times N$ symmetric random matrix $\boldsymbol{X}$. The empirical spectral density of $\boldsymbol{X}$ is defined as

$$\rho_X(\lambda) = \lim_{N\to\infty} \frac{1}{N} \sum_{j=1}^{N} \langle \delta(\lambda - \lambda_j(\boldsymbol{X})) \rangle, \tag{22}$$

with $\langle \ldots \rangle$ representing the average over the random-matrix ensemble. Introducing the $N \times N$ resolvent matrix

$$\boldsymbol{G}_X(z) = (z\boldsymbol{I} - \boldsymbol{X})^{-1} \tag{23}$$

associated to $\boldsymbol{X}$, we obtain $\rho_X(\lambda)$ from the resolvent as follows [50]

$$\rho_X(\lambda) = \lim_{\epsilon\to 0^+} \lim_{N\to\infty} \frac{1}{\pi N} \mathrm{Im} \langle \mathrm{Tr}\, \boldsymbol{G}_X(z) \rangle, \tag{24}$$

where $z = \lambda - i\epsilon$.

In the present work, the randomness stems from both heterogeneous temperatures $T_1, \ldots, T_N$ and random couplings K_{ij} (see section III). In appendix A, we explain how to calculate the ensemble average $\langle \mathrm{Tr}\, \boldsymbol{G}_{S^{-1}}(z) \rangle$ for the precision matrix $\boldsymbol{S}^{-1}$ using the replica method [47]. The spectral density of $\boldsymbol{S}^{-1}$ is given by

$$\rho_{S^{-1}}(\lambda) = \frac{1}{\pi} \lim_{\epsilon\to 0^+} \mathrm{Im} \left[\int_0^\infty dT \frac{p(T)}{\left(z - \frac{\mu}{T} - g^2(T) q\right)} \right], \tag{25}$$

where the replica-symmetric order-parameter q fulfills the self-consistent equation

$$q = \int_0^\infty dT \frac{p(T) g^2(T)}{\left(z - \frac{\mu}{T} - g^2(T) q\right)}. \tag{26}$$

Therefore, once we specify the function $g(T)$ and the distribution $p(T)$ of heterogeneous temperatures, we can solve the fixed-point Eq. (26) and determine $\rho_{S^{-1}}(\lambda)$. Given that $\lambda_i(\boldsymbol{S}) = 1/\lambda_i(\boldsymbol{S}^{-1})$ $(i = 1, \ldots, N)$, the spectral density $\rho_S(\lambda)$ of the stationary covariance matrix $\boldsymbol{S}$ follows from

$$\rho_S(\lambda) = \frac{1}{\lambda^2} \rho_{S^{-1}}(1/\lambda). \tag{27}$$

Clearly, to determine $\rho_S(\lambda)$, we must solve Eq. (26) at $z = 1/\lambda - i\epsilon$.

Comparing Eqs. (19) and (21), we note that $\boldsymbol{A}'$ and $\boldsymbol{S}^{-1}$ have a similar form. Hence, the replica method in appendix A can be applied in an analogous way to determine the spectral density $\rho_{A'}(\lambda)$ of the transformed interaction matrix $\boldsymbol{A}'$. The final outcome for $\rho_{A'}(\lambda)$ reads

$$\rho_{A'}(\lambda) = \frac{1}{\pi} \lim_{\epsilon\to 0^+} \mathrm{Im} \left[\int_0^\infty dT \frac{p(T)}{(z - \mu - T g^2(T) q)} \right], \tag{28}$$

where q solves the equation

$$q = \int_0^\infty dT \frac{p(T) T g^2(T)}{(z - \mu - T g^2(T) q)}. \tag{29}$$

According to Eq. (13), the function $\rho_{A'}(\lambda)$ determines the spectral density $\rho_{S'(\tau)}(\lambda)$ of the lagged covariance matrix $\boldsymbol{S}'(\tau)$. Indeed, since $\lambda_j(\boldsymbol{S}'(\tau)) = e^{-\tau\lambda_j(\boldsymbol{A}')}/\lambda_j(\boldsymbol{A}')$ $(j = 1, \ldots, N)$, we find the relation

$$\rho_{S'(\tau)}(\lambda) = \frac{\lambda'}{\lambda(1 + \tau\lambda')} \rho_{A'}(\lambda'), \tag{30}$$

where $\lambda' = \lambda'(\lambda)$ is determined from the solutions of the fixed-point equation

$$e^{-\tau\lambda'} = \lambda\lambda'. \tag{31}$$

V. RESULTS

In this section, we discuss our results for the spectral density of both lagged and stationary covariance matrices obtained from Eqs. (27) and (30). In order to solve the equations for the spectral densities, we need to specify the function $g(T)$ and the distribution $p(T)$ of temperatures. Here, we choose $g(T) = T^{-\alpha}$, with $\alpha \in [0, 1]$, and the entries of the coupling matrices $\boldsymbol{A}$ and $\boldsymbol{A'}$ assume the form

$$A_{ij} = \mu\delta_{ij} + T_i^{1-\alpha} K_{ij} T_j^{-\alpha}, \tag{32}$$

$$A'_{ij} = \mu\delta_{ij} + T_i^{\frac{1}{2}-\alpha} K_{ij} T_j^{\frac{1}{2}-\alpha}. \tag{33}$$

The matrix $\boldsymbol{A}$ is asymmetric, with A_{ij} representing the interaction strength or influence of $X_j(t)$ on $X_i(t)$. The exponent α shapes the role of the local temperatures on the pairwise interactions. For instance, when $\alpha = 1$, A_{ij} is weighted by $1/T_j$, which means that a variable $X_j(t)$ with a high temperature T_j will have a weak influence on the rest of the system.

We are also interested in the stability of MVOU processes. The dynamics of Eq. (1) evolves to stable stationary states if all eigenvalues of the precision matrix $\boldsymbol{S}^{-1}$ are non-negative [44, 45]. If we order these eigenvalues as $\lambda_1(\boldsymbol{S}^{-1}) < \lambda_2(\boldsymbol{S}^{-1}) < \cdots < \lambda_N(\boldsymbol{S}^{-1})$, MVOU processes are stable provided $\lambda_1(\boldsymbol{S}^{-1}) \geq 0$. Therefore, the lower spectral edge of $\rho_{S^{-1}}(\lambda)$ determines whether the system is stable in the limit $N \to \infty$. At marginal stability, the lower spectral edge of $\rho_{S^{-1}}(\lambda)$ touches zero, and the decay of $\rho_S(\lambda)$ for large λ is obtained from the functional behavior of $\rho_{S^{-1}}(\lambda)$ as $\lambda \to 0^+$ (see Eq. (27)).

We can also characterize the stability of MVOU processes in terms of the macroscopic parameter

$$m(t) = \lim_{N\to\infty} \frac{1}{N} \sum_{i=1}^{N} \langle X_i(t) \rangle_\eta \,. \tag{34}$$

For a stable MVOU process ($\lambda_1(\boldsymbol{S}^{-1}) \geq 0$), $m(t)$ relaxes to the trivial fixed-point $m = 0$. Conversely, for an unstable MVOU process, $m(t)$ diverges. Below, we present results for an homogeneous temperature and two cases of heterogeneous temperatures: a bimodal and a uniform distribution $p(T)$.

A. Homogeneous temperatures

Let us consider the analytically solvable case of a homogeneous temperature [45, 51], where $T_i = T \ \forall i$. Substituting $p(T') = \delta(T' - T)$ in Eq. (26) and solving the resulting quadratic equation for q, we obtain

$$q = \frac{1}{2g^2(T)} \left(z - \frac{\mu}{T} + \sqrt{\left(\frac{\mu}{T} - z\right)^2 - \Lambda^2} \right), \tag{35}$$

with $\Lambda = 2g^2(T)$. Inserting this result into Eq. (25) and taking the limit $\epsilon \to 0^+$, we derive the Wigner semicircle law for the spectral density of the precision matrix,

$$\rho_{S^{-1}}(\lambda) = \begin{cases} \dfrac{2}{\pi\Lambda^2} \sqrt{\Lambda^2 - \left(\dfrac{\mu}{T} - \lambda\right)^2} & \text{if } \ \lambda \in (\lambda_-, \lambda_+)\,, \\ 0 & \text{otherwise,} \end{cases} \tag{36}$$

where the spectral edges read $\lambda_\pm = \frac{\mu}{T} \pm \Lambda$. For stable MVOU processes, where $\lambda_- > 0$, the spectral density of $\boldsymbol{S}$ is given by

$$\rho_S(\lambda) = \begin{cases} \dfrac{2}{\pi\Lambda^2\lambda^2} \sqrt{\Lambda^2 - \left(\dfrac{\mu}{T} - \dfrac{1}{\lambda}\right)^2} & \text{if } \ \lambda \in \left(\lambda_+^{-1}, \lambda_-^{-1}\right), \\ 0 & \text{otherwise.} \end{cases} \tag{37}$$

The above expression, which follows from Eqs. (27) and (36), has been derived in previous works [45, 51].

We note that $\rho_S(\lambda)$ has a bounded support if the MVOU process is stable ($\lambda_- > 0$). However, as the system approaches marginal stability ($\lambda_- \to 0^+$), the support becomes unbounded and the distribution $\rho_S(\lambda)$ develops a power-law tail $\rho_S(\lambda) \propto \lambda^{-5/2}$ for large λ. This means that the variables $X_1(t), \ldots, X_N(t)$ are strongly correlated at marginal stability. In Fig. 1, we illustrate the behavior of $\rho_{S^{-1}}(\lambda)$ and $\rho_S(\lambda)$ across the stability transition. By setting $\lambda_- = 0$, we find the critical value $\mu_c = T\Lambda$ at which the system is marginally stable. We also point out that the shape of $\rho_S(\lambda)$ is similar to the one in [7], with the difference that our results follow from a random-matrix model for the interaction matrix $\boldsymbol{A}$, while in [7] the spectral density of $\boldsymbol{S}$ is derived from the Wishart random-matrix ensemble.

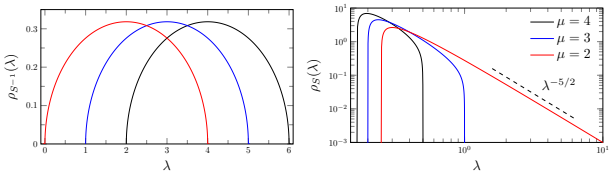

FIG. 1. Spectral density of the precision matrix $\boldsymbol{S}^{-1}$ (Eq. (36)) and of the covariance matrix $\boldsymbol{S}$ for stationary MVOU processes interacting through Eq. (32) with $\alpha = 1$. The temperatures are equal to $T_i = 1 \ \forall i$. In the stable regime ($\mu > 2$), the spectral density $\rho_S(\lambda)$ is given by Eq. (37), while it exhibits a power-law tail at marginal stability ($\mu = 2$).

From Eqs. (28) and (29), one can show that $\rho_{A'}(\lambda)$ also follows the Wigner semicircle law, which yields the spectral density of the lagged covariance matrix $S'(\tau)$ of the stable MVOU process described by Eq. (11),

$$\rho_{S'(\tau)}(\lambda) = \begin{cases} F(\lambda, \lambda') \sqrt{T^2\Lambda^2 - (\mu - \lambda')^2} & \text{if } \lambda \in (\gamma_+, \gamma_-) \\ 0 & \text{otherwise.} \end{cases} \tag{38}$$

The function $F(\lambda, \lambda')$ is defined as

$$F(\lambda, \lambda') = \frac{2\lambda'}{\pi\Lambda^2 T^2 \lambda(1 + \tau\lambda')}, \tag{39}$$

while the variable λ' solves Eq. (31). The upper and lower spectral edges of $\rho_{S'(\tau)}(\lambda)$ are given by

$$\gamma_{\pm} = \frac{\exp\left[-\tau\left(\mu \pm T\Lambda\right)\right]}{\mu \pm T\Lambda}. \tag{40}$$

The finite and positive support of $\rho_{S'(\tau)}(\lambda)$ reflects the stability of the MVOU process.

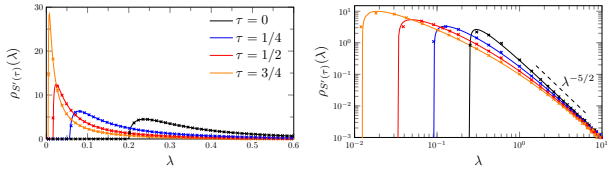

FIG. 2. Spectral density $\rho_{S'(\tau)}(\lambda)$ of the lagged covariance matrix $\boldsymbol{S}'(\tau)$ for stationary MVOU processes described by Eq. (11). The coupling matrix is given by Eq. (33), with $\alpha = 1$ and a homogeneous temperature $T_i = 1\ \forall i$. The left panel shows $\rho_{S'(\tau)}(\lambda)$ in the stable regime ($\mu = 3$), while the right panel illustrates the power-law decay of $\rho_{S'(\tau)}(\lambda)$ at marginal stability ($\mu = 2$). The solid lines are obtained from Eq. (38), while the symbols are numerical diagonalization results derived from an ensemble of 10 matrices $\boldsymbol{S}'(\tau)$ with $N = 10^4$.

As $\mu \to \mu_c^+$, the upper spectral edge γ_- diverges, and $\rho_{S'(\tau)}(\lambda)$ decays as $\rho_{S'(\tau)}(\lambda) \propto \lambda^{-5/2}$ for large λ. Figure 2 illustrates the effect of the time-difference τ on the spectral density $\rho_{S'(\tau)}(\lambda)$ for both stable ($\mu > \mu_c$) and marginally stable ($\mu = \mu_c$) MVOU processes. As τ increases, $\rho_{S'(\tau)}(\lambda)$ develops a peak close to $\lambda = 0$, corresponding to uncorrelated dynamical variables in the stationary state. In the marginally stable regime, $\rho_{S'(\tau)}(\lambda)$ also exhibits an excess of modes around zero, but large correlations among the dynamical variables lead to the power-law decay in $\rho_{S'(\tau)}(\lambda)$. For $\tau \to 0$, $\rho_{S'(\tau)}(\lambda)$ converges to the spectral density of the equal-time covariance $\boldsymbol{S}'$, which characterizes the stationary states of Eq. (11).

B. Bimodal temperature distribution

In this subsection, we present results for the bimodal distribution of temperatures

$$p_{\rm b}(T) = p\delta(T - T_0) + (1-p)\delta(T - T_0 - \delta), \tag{41}$$

with $T_0 > 0$ and $\delta > 0$. The parameter $p \in [0,1]$ determines the fraction of dynamical variables $\{X_i(t)\}_{i=1,\ldots,N}$ in the lowest temperature T_0. Below, we exploit how bimodal temperatures impact the stability transition of MVOU processes and the spectral densities of the covariance matrices.

For heterogeneous temperatures, where the variance of $p(T)$ is finite, we obtain the spectral densities of $\boldsymbol{S}$ and $\boldsymbol{S}'(\tau)$ by numerically solving the self-consistent Eqs. (26) and (29), respectively. In Fig. 3, we compare numerical diagonalization results with our theoretical findings for $\rho_S(\lambda)$ and $\rho_{S'(\tau)}(\lambda)$ in the limit $N \to \infty$. The excellent agreement between the two approaches validates our theoretical predictions. The results in Fig. 3 are for stable MVOU processes, where $\rho_S(\lambda)$ is supported on a finite, positive interval.

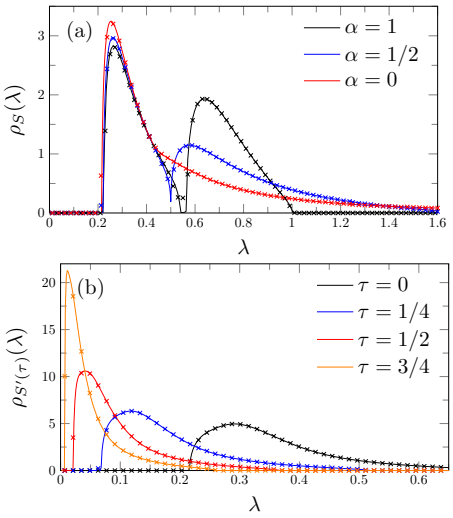

FIG. 3. (a) Spectral density $\rho_S(\lambda)$ of the covariance matrix $\boldsymbol{S}$ for stationary MVOU processes interacting through Eq. (32) with $\mu = 3$ and different values of α. (b) Spectral density $\rho_{S'(\tau)}(\lambda)$ of the lagged covariance matrix $S'(\tau)$ for stationary MVOU processes (see Eq. (11)) interacting through Eq. (33) with $\alpha = 1$ and $\mu = 3$. The temperatures in both panels follow a bimodal distribution with $T_0 = \delta = 1$ and $p = 1/2$ (see Eq. (41)). The solid lines are obtained from the solutions of Eqs. (26) and (29) with $\epsilon = 10^{-3}$, while the symbols are numerical diagonalization results derived from an ensemble of 10 covariance matrices with $N = 10^4$.

As μ decreases, MVOU processes interacting through Eq. (32) become unstable. Figure 4 shows the stability diagram (μ, p) for $\alpha = 1$ and a bimodal temperature distribution. Since for $\alpha = 1$ the couplings A_{ij} are weighted by $1/T_j$, the system becomes more stable as p decreases, due to the larger number of weaker interactions among the dynamical variables. For the same reason, a larger temperature difference δ also promotes stability. The system is marginally stable at the solid lines, which are determined by the values of (μ, p) where the lower spectral edge of $\rho_{S^{-1}}(\lambda)$ is zero. The inset in Fig. 4 shows numerical simulations confirming that the macroscopic variable $m(t)$ relaxes to zero when the system is stable, while it diverges in the unstable regime.

The lower panels in Fig. 4 show the behavior of the spectral densities $\rho_S(\lambda)$ and $\rho_{S^{-1}}(\lambda)$ across the stability transition. In the stable regime, $\rho_S(\lambda)$ is supported on a finite interval and it exhibits two maxima, reflecting the bimodal shape of $p_{\rm b}(T)$. At marginal stability, we have numerically confirmed that $\rho_{S^{-1}}(\lambda) \propto \sqrt{\lambda}$ as $\lambda \to 0^+$, independently of α. This behavior leads to an unbounded density $\rho_S(\lambda)$ with a power-law tail $\rho_S(\lambda) \propto \lambda^{-5/2}$ for large λ.

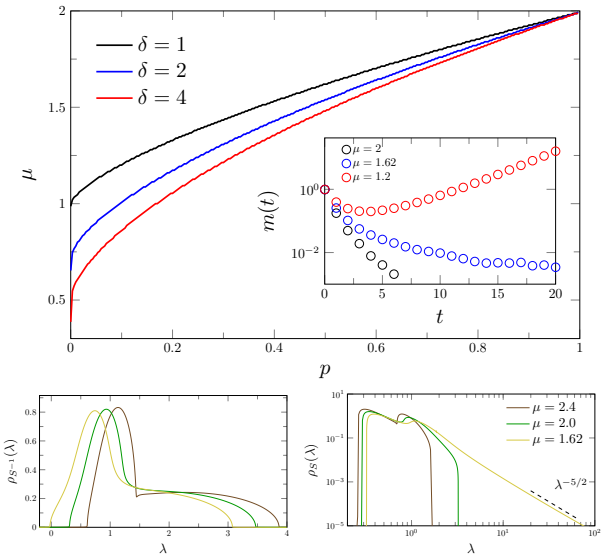

FIG. 4. Main panel: stability diagram (μ, p) of stationary MVOU processes with $\alpha = 1$ (see Eq. (32)). The temperatures are drawn from the bimodal distribution of Eq. (41) with $T_0 = 1$. The MVOU process is stable above the solid lines, unstable below them, and marginally stable at the lines. The inset displays the dynamics of $m(t)$, Eq. (34), for $p = 1/2$, $\delta = 1$, and different μ. These results follow from the numerical integration of Eq. (1) for an ensemble of $N = 10^3$ dynamical variables. Lower panels: spectral densities of the covariance and precision matrices, $\boldsymbol{S}$ and $\boldsymbol{S}^{-1}$, across the stability transition for $T_0 = \delta = 1$ and $p = 1/2$. These results are obtained from the solutions of Eq. (26) with $\epsilon = 10^{-6}$.

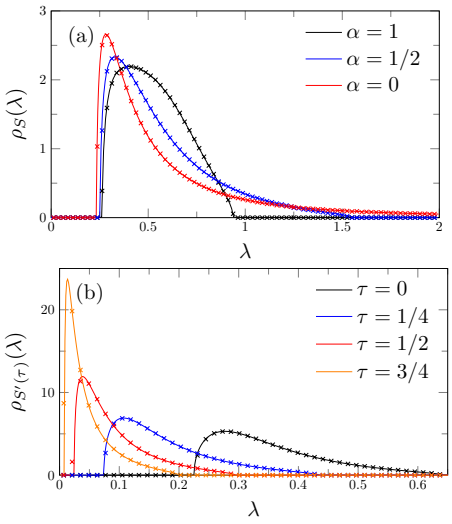

FIG. 5. (a) Spectral density $\rho_S(\lambda)$ of the covariance matrix $\boldsymbol{S}$ for stationary MVOU processes interacting through Eq. (32) with $\mu = 3$ and different α. (b) Spectral density $\rho_{S'(\tau)}(\lambda)$ of the lagged covariance matrix $S'(\tau)$ for stationary MVOU processes (see Eq. (11)) interacting through Eq. (33) with $\alpha = 1$ and $\mu = 3$. The temperatures in both panels follow an uniform distribution with $T_M = 3/2$ and $\Delta = 1$ (see Eq. (42)). The solid lines are derived from the solutions of Eqs. (26) and (29) with $\epsilon = 10^{-3}$, while the symbols are numerical diagonalization results obtained from an ensemble of 10 covariance matrices with $N = 10^4$.

C. Uniform temperature distribution

In this subsection, we derive results for the uniform distribution of temperatures

$$p_{\rm u}(T) = \begin{cases} \Delta^{-1} & \text{if } \; T \in (T_M - \Delta/2, T_M + \Delta/2)\,, \\ 0 & \text{otherwise,} \end{cases} \tag{42}$$

where $T_M > 0$ and $\Delta \in (0, 2\,T_M)$ are, respectively, the center and the width of $p_{\rm u}(T)$. In Fig. 5, we compare our analytic results for $\rho_S(\lambda)$ and $\rho_{S'(\tau)}(\lambda)$ with numerical diagonalization results of finite covariance matrices for temperatures drawn from Eq. (42). The results in Fig. 5 once more confirm the exactness of our theoretical findings for $N \to \infty$.

Figure 6 shows the stability diagram (μ, Δ) for stationary MVOU processes interacting according to Eq. (32) with $\alpha = 1$. The temperatures follow the uniform distribution specified in Eq. (42). As the width Δ increases towards its maximum $2\,T_M$, the system becomes less stable, due to the growing number of strong pairwise couplings arising from small temperatures. Additionally, Fig. 6 illustrates the evolution of $\rho_S(\lambda)$ and $\rho_{S^{-1}}(\lambda)$ as Δ increases from the stable regime to the marginal stability line. The effect of increasing temperature fluctuations is to broaden the support of the spectral densities. At marginal stability, $\rho_S(\lambda)$ exhibits once more the power-law tail $\rho_S(\lambda) \propto \lambda^{-5/2}$, due to the functional behavior $\rho_{S^{-1}}(\lambda) \propto \sqrt{\lambda}$ close to the lower spectral edge $\lambda = 0$.

VI. DISCUSSION

We have introduced a random matrix model for covariance matrices of reversible multivariate Ornstein-Uhlenbeck processes (MVOU), in which the ensemble is constrained by the solutions of the Sylvester-Lyapunov equation. In contrast to traditional random-matrix ensembles of the covariance [7, 31, 32], where the statistics of the matrix elements is independent of the interactions and diffusion terms, here the covariance naturally follows from the distribution of coupling strengths and temperatures characterizing MVOU processes, representing an alternative family of null models for the empirical correlations in stochastic complex systems. In addition, by making a linear transformation of the dynamical variables, we have shown how the lagged covariance matrix becomes a simple function of the coupling matrix in the transformed system. Thus, our ensemble enables to study the effect of random interactions and heterogeneous temperatures on the spectral density of both the equal-time covariance and the lagged covariance matrices that characterize the stationary states of reversible MVOU processes.

Building on the replica method of spin-glass theory

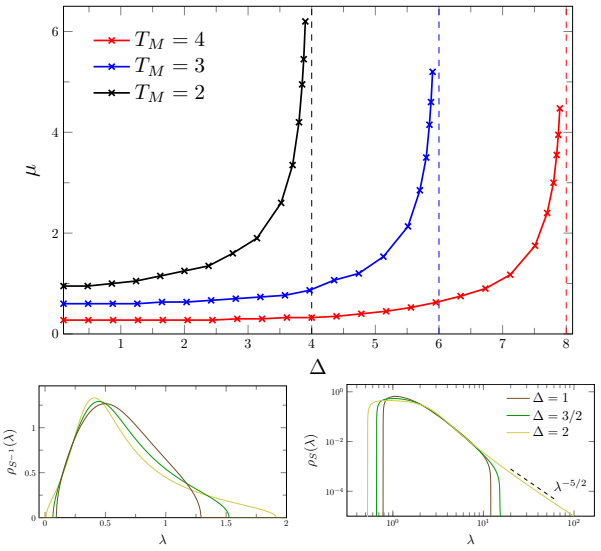

FIG. 6. Main panel: stability diagram (μ, Δ) of stationary MVOU processes with $\alpha = 1$ (see Eq. (32)). The temperatures follow the uniform distribution of Eq. (42). The symbols identify points of the stability transition, while the solid lines are a guide to the eye. The vertical dashed lines mark the maximum value $\Delta = 2T_M$. The MVOU process is stable above the transition points, unstable below them, and marginally stable at the points. Lower panels: spectral densities of the covariance and precision matrices, $\boldsymbol{S}$ and $\boldsymbol{S}^{-1}$, for $T_M = 2$, $\mu = 1.2$, and increasing values of Δ. These results are obtained from the solutions of Eq. (26) with $\epsilon = 10^{-6}$.

[47], we have derived an exact equation for the spectral density of the equal-time covariance matrix of the stationary states. We have shown that the stationary states undergo a transition between stability and instability, which manifests itself on the shape of the spectral density. In the stable regime, all eigenvalues of the covariance are positive and its spectral density is bounded, while negative eigenvalues emerge in the unstable phase. Interestingly, at marginal stability, the spectral density $\rho_S(\lambda)$ becomes unbounded, decaying as a power-law $\rho_S(\lambda) \propto \lambda^{-5/2}$ for large eigenvalues. The exponent of the power-law tail is independent of the details defining the model, such as the distribution of temperatures, indicating an universal behavior of the covariance at marginal stability. Based on the spectral properties of the covariance matrix, we have derived phase diagrams that illustrate how temperature fluctuations influence the stability of the system.

The flexibility of the model introduced here allows to explore how more structured interactions in MVOU processes influence the spectral density of the covariance matrix. An important question in this context is whether the general features of the spectral density across the stability transition remain valid in the more realistic scenario of sparse interactions [50]. Additionally, to establish the power-law decay as a robust property of the covariance spectral density, it is crucial to understand how both the breakdown of Onsager reversibility and the nonlinearity in the dynamics of complex systems [20, 23, 24] affect the spectral properties of the covariance at marginal stability. Finally, we highlight that our random-matrix ensemble offers an alternative null model for the empirical covariance of complex systems. We hope this will stimulate comparisons between our theoretical predictions and empirical data.

ACKNOWLEDGMENTS

L. S. F. acknowledges a fellowship from CNPq/Brazil. F. L. M. thanks CNPq/Brazil for financial support.

Appendix A: Replica method for the spectral density of the precision matrix

In this appendix, we explain how to employ the replica method of disordered systems to obtain an analytic expression for the spectral density of the precision matrix $\boldsymbol{S}^{-1}$ in the limit $N \to \infty$. The derivation of the spectral density of the transformed matrix $\boldsymbol{A}'$ is completely analogous, and here we will state only the final result.

Let us introduce the $N \times N$ resolvent matrix of $\boldsymbol{S}^{-1}$,

$$\boldsymbol{G}_{S^{-1}}(z) = (z\boldsymbol{I} - \boldsymbol{S}^{-1})^{-1}, \tag{A1}$$

where $\boldsymbol{I}$ is the identity matrix and $z = \lambda - i\epsilon$, with the regularizer $\epsilon > 0$. The precision matrix is defined in Eq. (21). The empirical spectral density of $\boldsymbol{S}^{-1}$ follows from

$$\rho_{S^{-1}}(\lambda) = \lim_{\epsilon \to 0^+} \lim_{N \to \infty} \frac{1}{\pi N} \mathrm{Im} \left\langle \mathrm{Tr}\, \boldsymbol{G}_{S^{-1}}(z) \right\rangle, \tag{A2}$$

with $\langle \dots \rangle$ denoting the ensemble average over the temperatures $T_1, \dots, T_N$ and the off-diagonal entries of $\boldsymbol{K}$. The latter follow a Gaussian distribution with mean zero and variance $1/N$.

To proceed further, we map the problem of computing the ensemble average $\langle \mathrm{Tr}\, \boldsymbol{G}_{S^{-1}}(z) \rangle$ into a statistical mechanics calculation [52]. By using the identity

$$\mathrm{Tr}\boldsymbol{G}_{S^{-1}}(z) = -2\frac{\partial}{\partial z} \ln \left[\det\left(z\boldsymbol{I} - \boldsymbol{S}^{-1}\right)\right]^{-1/2}, \tag{A3}$$

and representing $\left[\det\left(z - \boldsymbol{S}^{-1}\right)\right]^{-1/2}$ as a Gaussian integral over real variables $\boldsymbol{\phi} = (\phi_1, \dots \phi_N)^T$, we rewrite the above expression as

$$\mathrm{Tr}\boldsymbol{G}_{S^{-1}}(z) = -2\frac{\partial}{\partial z} \ln \mathcal{Z}(z), \tag{A4}$$

where

$$\mathcal{Z}(z) = \int_{-\infty}^{\infty} \left(\prod_{j=1}^{N} d\phi_j \right) \exp\left[-\frac{i}{2} \boldsymbol{\phi}^T \left(z\boldsymbol{I} - \boldsymbol{S}^{-1} \right) \boldsymbol{\phi} \right] \tag{A5}$$

is the partition function associated to the random-matrix model. Thus, the problem of computing the ensemble average $\langle \mathrm{Tr}\, \boldsymbol{G}_{S^{-1}}(z)\rangle$ boils down to calculate the averaged free-energy $\langle \ln \mathcal{Z}(z)\rangle$.

To calculate the average over the random-matrix ensemble, we use the replica method [47], which is based on the following identity

$$\langle \ln \mathcal{Z}(z)\rangle = \lim_{n\to 0} \frac{1}{n} \ln \langle \mathcal{Z}^n(z)\rangle. \tag{A6}$$

The strategy is to compute first the average $\langle \mathcal{Z}^n(z)\rangle$ for a positive integer n, and then reconstruct $\langle \ln \mathcal{Z}(z)\rangle$ by taking the limit $n \to 0$, according to Eq. (A6). By substituting Eq. (21) in Eq. (A5) and then performing the average of the replicated partition function $\mathcal{Z}^n(z)$ over the Gaussian distributed off-diagonal elements K_{ij}, we obtain

$$\langle \mathcal{Z}^n(z)\rangle \simeq \left\langle \left(\prod_{j=1}^{N} d\boldsymbol{\phi}_j\right) \exp\left[-\frac{i}{2}\sum_{i=1}^{N}\left(z-\frac{\mu}{T_i}\right)\boldsymbol{\phi}_i^2\right] \times \exp\left[-\frac{N}{4}\sum_{\alpha,\beta=1}^{n}\left(\frac{1}{N}\sum_{i=1}^{N} g^2(T_i)\phi_i^\alpha \phi_i^\beta\right)^2\right]\right\rangle_{T_1,\ldots,T_N}, \tag{A7}$$

where $\boldsymbol{\phi}_i = (\phi_i^1, \ldots, \phi_i^n)^T$ is the n-dimensional vector in the replica space, and $\langle \ldots \rangle_{T_1,\ldots,T_N}$ represents the average over the temperatures $T_1, \ldots, T_N$. We have neglected terms of $O(N^0)$ in the exponent of Eq. (A7), since these are subleading contributions in the limit $N \to \infty$. Using the Hubbard-Stratonovich transformation,

$$\sqrt{\pi N}\exp\left[-\frac{N}{4}\left(\frac{1}{N}\sum_{i=1}^{N} g^2(T_i)\phi_i^\alpha\phi_i^\beta\right)^2\right] = \int dq_{\alpha\beta}\, \exp\left(-\frac{q_{\alpha\beta}^2}{N} + \frac{i q_{\alpha\beta}}{N}\sum_{i=1}^{N} g^2(T_i)\phi_i^\alpha\phi_i^\beta\right), \tag{A8}$$

we introduce the order-parameters $\{q_{\alpha\beta}\}_{\alpha,\beta=1,\ldots,N}$, which enables to decouple the variables $\boldsymbol{\phi}_1, \ldots, \boldsymbol{\phi}_N$ at different sites. Additionally, by rescaling $q_{\alpha\beta}$ as $q_{\alpha\beta} \to N q_{\alpha\beta}$, we can rewrite Eq. (A7) as follows

$$\langle \mathcal{Z}^n(z)\rangle \simeq \int \left(\prod_{\alpha,\beta=1}^{n} dq_{\alpha\beta}\right) e^{-N\Phi(\{q_{\alpha\beta}\})}, \tag{A9}$$

where

$$\Phi(\{q_{\alpha\beta}\}) = \sum_{\alpha,\beta=1}^{n} q_{\alpha\beta}^2 - \ln\left\langle \int d\boldsymbol{\phi}\, e^{H_T(\boldsymbol{\phi})}\right\rangle_T. \tag{A10}$$

The function $H_T(\boldsymbol{\phi})$,

$$H_T(\boldsymbol{\phi}) = -\frac{i}{2}\left(z-\frac{\mu}{T}\right)\boldsymbol{\phi}^2 + i g^2(T)\sum_{\alpha,\beta=1}^{n} q_{\alpha\beta}\phi^\alpha\phi^\beta, \tag{A11}$$

can be interpreted as an effective single-site Hamiltonian. When writing Eq. (A9), we have ignored constants that do not contribute to $\langle \mathcal{Z}^n(z)\rangle$ in the limit $N \to \infty$.

We can now evaluate the integral in Eq. (A9) using the saddle-point method. In the limit $N \to \infty$, $\langle \mathcal{Z}^n(z)\rangle$ is asymptotically given by

$$\langle \mathcal{Z}^n(z)\rangle \sim e^{-N\Phi(\{q_{\alpha\beta}\})}, \tag{A12}$$

where the order-parameters $\{q_{\alpha\beta}\}_{\alpha,\beta=1,\ldots,N}$ fulfill the saddle-point equations

$$q_{\alpha\beta} = \frac{i}{2}\frac{\left\langle g^2(T)\int d\boldsymbol{\phi}\, \phi^\alpha\phi^\beta e^{H_T(\boldsymbol{\phi})}\right\rangle_T}{\left\langle \int d\boldsymbol{\phi}\, e^{H_T(\boldsymbol{\phi})}\right\rangle_T}. \tag{A13}$$

The above equation is obtained by imposing the stationarity condition $\frac{\partial \Phi}{\partial q_{\alpha\beta}} = 0$ on $\Phi(\{q_{\alpha\beta}\})$. Combining Eq. (A12) with Eqs. (A2) and (A6), we obtain an expression for the spectral density in terms of $\Phi(\{q_{\alpha\beta}\})$, that is

$$\rho_{S^{-1}}(\lambda) = \frac{2}{\pi}\lim_{\epsilon\to 0^+}\mathrm{Im}\left[\frac{\partial}{\partial z}\lim_{n\to 0}\Phi(\{q_{\alpha\beta}\})\right]. \tag{A14}$$

Finally, we simplify the saddle-point equations by making the diagonal replica symmetric *ansatz*

$$q_{\alpha\beta} = \frac{q}{2}\delta_{\alpha\beta} \quad (q \in \mathbb{C}). \tag{A15}$$

Inserting the above assumption into Eqs. (A13) and (A14) and taking the limit $n \to 0$, we arrive at the final expression for the spectral density

$$\rho_{S^{-1}}(\lambda) = \frac{1}{\pi}\lim_{\epsilon\to 0^+}\mathrm{Im}\left\langle \frac{1}{z-\frac{\mu}{T}-g^2(T)q}\right\rangle_T \tag{A16}$$

where q solves the fixed-point equation

$$q = \left\langle \frac{g^2(T)}{z-\frac{\mu}{T}-g^2(T)q}\right\rangle_T. \tag{A17}$$

The application of the replica method to determine the spectral density $\rho_{A'}(\lambda)$ of the transformed coupling matrix $\boldsymbol{A'}$ unfolds in a similar way. By comparing Eqs. (19) and (21), it is straightforward to conclude that $\rho_{A'}(\lambda)$ is given by

$$\rho_{A'}(\lambda) = \frac{1}{\pi}\lim_{\epsilon\to 0^+}\mathrm{Im}\left\langle \frac{1}{z-\mu-Tg^2(T)q}\right\rangle_T, \tag{A18}$$

where q fulfills the equation

$$q = \left\langle \frac{Tg^2(T)}{z-\mu-Tg^2(T)q}\right\rangle_T. \tag{A19}$$

Appendix B: Bounds on the largest and smallest eigenvalues of the lagged covariance

The introduction of a rescaled system with transformed interaction matrix $\boldsymbol{A'}$ and transformed lagged covariance $\boldsymbol{S'}(\tau)$ provides a set of relations that we cannot

simply derive in the original basis. In section V, we obtain the full spectrum of $\boldsymbol{S}'(\tau)$ for any τ, which allows us to set a few bounds on the eigenvalues of the original lagged covariance $\boldsymbol{S}(\tau)$, thanks to Eq. (15). In fact, given two positive-definite invertible matrices [48, 49], $\boldsymbol{P}$ and $\boldsymbol{Q}$, the following inequalities hold

$$\lambda_{\max}(\boldsymbol{P})\lambda_{\min}(\boldsymbol{Q}) \leq \lambda_{\max}(\boldsymbol{PQ}) \leq \lambda_{\max}(\boldsymbol{P})\lambda_{\max}(\boldsymbol{Q}), \tag{B1}$$

$$\lambda_{\min}(\boldsymbol{P})\lambda_{\min}(\boldsymbol{Q}) \leq \lambda_{\min}(\boldsymbol{PQ}) \leq \lambda_{\min}(\boldsymbol{P})\lambda_{\max}(\boldsymbol{Q}), \tag{B2}$$

where $\lambda_{\max}$ and $\lambda_{\min}$ denote, respectively, the largest and the smallest eigenvalue of the corresponding matrices. In our case, as the diffusion matrix is given by $D_{ij} = T_i\delta_{ij}$, we can apply the above relationships to Eq. (15) and obtain bounds for the spectrum of $\boldsymbol{S}(\tau)$,

$$T^2_{\min}\lambda_{\max}(\boldsymbol{S}'(\tau)) \leq \lambda_{\max}(\boldsymbol{S}(\tau)) \leq T^2_{\max}\lambda_{\max}(\boldsymbol{S}'(\tau)), \tag{B3}$$

$$T^2_{\min}\lambda_{\min}(\boldsymbol{S}'(\tau)) \leq \lambda_{\min}(\boldsymbol{S}(\tau)) \leq T^2_{\max}\lambda_{\min}(\boldsymbol{S}'(\tau)), \tag{B4}$$

where $T_{\max}$ and $T_{\min}$ are the largest and smallest temperatures, respectively. Further bounds can be also obtained for the intermediate eigenvalues [48].

[1] C. A Tracy and H. Widom, "The distributions of random matrix theory and their applications," in *New Trends in Mathematical Physics: Selected contributions of the XVth International Congress on Mathematical Physics* (Springer, 2009) pp. 753–765.

[2] E. P. Wigner, "On the distribution of the roots of certain symmetric matrices," Annals of Mathematics **67**, 325–327 (1958).

[3] A. D. Mirlin, "Statistics of energy levels and eigenfunctions in disordered systems," Physics Reports **326**, 259 – 382 (2000).

[4] E. F. N. Santos, A. L. R. Barbosa, and P. J. Duarte-Neto, "Global correlation matrix spectra of the surface temperature of the oceans from random matrix theory to poisson fluctuations," Physics Letters A **384**, 126689 (2020).

[5] J. Kwapień, S. Drożdż, and A. A. Ioannides, "Temporal correlations versus noise in the correlation matrix formalism: an example of the brain auditory response," Physical Review E **62**, 5557 (2000).

[6] V. Plerou, P. Gopikrishnan, B. Rosenow, L. A. N. Amaral, and H. E. Stanley, "Universal and nonuniversal properties of cross correlations in financial time series," Physical review letters **83**, 1471 (1999).

[7] L. Laloux, P. Cizeau, J. Bouchaud, and M. Potters, "Noise dressing of financial correlation matrices," Phys. Rev. Lett. **83**, 1467–1470 (1999).

[8] D. Song, M. Tumminello, W. Zhou, and R. N. Mantegna, "Evolution of worldwide stock markets, correlation structure, and correlation-based graphs," Phys. Rev. E **84**, 026108 (2011).

[9] L. Sandoval and I. P. Franca, "Correlation of financial markets in times of crisis," Physica A: Statistical Mechanics and its Applications **391**, 187–208 (2012).

[10] M. C. Münnix, T. Shimada, R. Schäfer, F. Leyvraz, T. H. Seligman, T. Guhr, and H. E. Stanley, "Identifying states of a financial market," Sci. Rep. **2**, 644 (2012).

[11] O. Ledoit and M. Wolf, "A well-conditioned estimator for large-dimensional covariance matrices," Journal of multivariate analysis **88**, 365–411 (2004).

[12] J. Bun, J. Bouchaud, and M. Potters, "Cleaning large correlation matrices: Tools from random matrix theory," Physics Reports **666**, 1–109 (2017).

[13] Z. Burda and A. Jarosz, "Cleaning large-dimensional covariance matrices for correlated samples," Physical Review E **105**, 034136 (2022).

[14] F. L. Metz, "Dynamical mean-field theory of complex systems on sparse directed networks," (2024), arXiv:2406.06346 [cond-mat.dis-nn].

[15] Yan V. Fyodorov and Boris A. Khoruzhenko, "Nonlinear analogue of the may-wigner instability transition," Proceedings of the National Academy of Sciences **113**, 6827–6832 (2016), https://www.pnas.org/doi/pdf/10.1073/pnas.1601136113.

[16] Gérard Ben Arous, Yan V. Fyodorov, and Boris A. Khoruzhenko, "Counting equilibria of large complex systems by instability index," Proceedings of the National Academy of Sciences **118**, e2023719118 (2021), https://www.pnas.org/doi/pdf/10.1073/pnas.2023719118.

[17] R. M. May, "Will a large complex system be stable?" Nature **238**, 413–414 (1972).

[18] S. Allesina and S. Tang, "Stability criteria for complex ecosystems," Nature **483**, 205–208 (2012).

[19] Y. Krumbeck, Q. Yang, G. W. A. Constable, and T. Rogers, "Fluctuation spectra of large random dynamical systems reveal hidden structure in ecological networks," Nature Communications **12**, 3625 (2021).

[20] D. Martí, N. Brunel, and S. Ostojic, "Correlations between synapses in pairs of neurons slow down dynamics in randomly connected neural networks," Phys. Rev. E **97**, 062314 (2018).

[21] I. Neri and F. L. Metz, "Linear stability analysis of large dynamical systems on random directed graphs," Phys. Rev. Res. **2**, 033313 (2020).

[22] N. Patil, F. Aguirre-López, and J. Bouchaud, "The spectral boundary of block structured random matrices," Journal of Physics: Complexity **5**, 035001 (2024).

[23] H. Sompolinsky, A. Crisanti, and H. J. Sommers, "Chaos in random neural networks," Phys. Rev. Lett. **61**, 259–262 (1988).

[24] G. Bunin, "Ecological communities with lotka-volterra dynamics," Phys. Rev. E **95**, 042414 (2017).

[25] J. M. Beggs and D. Plenz, "Neuronal avalanches in neocortical circuits," Journal of Neuroscience **23**, 11167–11177 (2003), https://www.jneurosci.org/content/23/35/11167.full.pdf.

[26] Miguel A. Muñoz, "Colloquium: Criticality and dynamical scaling in living systems," Rev. Mod. Phys. **90**, 031001 (2018).

[27] J. Moran and J. Bouchaud, "May's instability in large economies," Phys. Rev. E **100**, 032307 (2019).

[28] Jean-Philippe Bouchaud, "The self-organized criticality paradigm in economics and finance," (2024), arXiv:2407.10284 [q-fin.GN].

[29] V. Plerou, P. Gopikrishnan, B. Rosenow, L. A. N. Amaral, T. Guhr, and H. E. Stanley, "Random matrix approach to cross correlations in financial data," Phys. Rev. E **65**, 066126 (2002).

[30] J. D. Noh, "Model for correlations in stock markets," Phys. Rev. E **61**, 5981–5982 (2000).

[31] Z. Burda, J. Jurkiewicz, M. A Nowak, G. Papp, and I. Zahed, "Free lévy matrices and financial correlations," Physica A: Statistical Mechanics and its Applications **343**, 694–700 (2004).

[32] Z. Burda, A. Görlich, A. Jarosz, and J. Jurkiewicz, "Signal and noise in correlation matrix," Physica A: Statistical Mechanics and its Applications **343**, 295–310 (2004).

[33] Z. Burda, J. Jurkiewicz, and B. Wacław, "Spectral moments of correlated wishart matrices," Physical Review E **71**, 026111 (2005).

[34] Z. Burda, A. Jarosz, M. A Nowak, and Małgorzata S., "A random matrix approach to varma processes," New Journal of Physics **12**, 075036 (2010).

[35] P. Barucca, M. Kieburg, and A. Ossipov, "Eigenvalue and eigenvector statistics in time series analysis," Europhysics Letters **129**, 60003 (2020).

[36] J. Wishart, "The generalised product moment distribution in samples from a normal multivariate population," Biometrika **20A**, 32–52 (1928), https://academic.oup.com/biomet/article-pdf/20A/1-2/32/530655/20A-1-2-32.pdf.

[37] V. A. Marchenko and L. A. Pastur, "Distribution of eigenvalues for some sets of random matrices," Matematicheskii Sbornik **114**, 507–536 (1967).

[38] E. Katzav and I. P. Castillo, "Large deviations of the smallest eigenvalue of the wishart-laguerre ensemble," Phys. Rev. E **82**, 040104 (2010).

[39] S. N. Majumdar and P. Vivo, "Number of relevant directions in principal component analysis and wishart random matrices," Phys. Rev. Lett. **108**, 200601 (2012).

[40] I. P. Castillo and F. L. Metz, "Large-deviation theory for diluted wishart random matrices," Phys. Rev. E **97**, 032124 (2018).

[41] C. Kwon, P. Ao, and D. J. Thouless, "Structure of stochastic dynamics near fixed points," Proceedings of the National Academy of Sciences **102**, 13029–13033 (2005), https://www.pnas.org/doi/pdf/10.1073/pnas.0506347102.

[42] H. Risken, *Fokker-planck equation* (Springer, 1996).

[43] A. Meucci, "Review of statistical arbitrage, cointegration, and multivariate ornstein-uhlenbeck," Cointegration, and Multivariate Ornstein-Uhlenbeck (May 14, 2009) (2009).

[44] C. Godrèche and J. Luck, "Characterising the nonequilibrium stationary states of ornstein–uhlenbeck processes," Journal of Physics A: Mathematical and Theoretical **52**, 035002 (2019).

[45] Y. V. Fyodorov, E. Gudowska-Nowak, M. A Nowak, and W. Tarnowski, "Fluctuation-dissipation relation for non-hermitian langevin dynamics," arXiv preprint arXiv:2310.09018 (2023).

[46] P. Barucca, "Localization in covariance matrices of coupled heterogeneous ornstein-uhlenbeck processes," Physical Review E **90**, 062129 (2014).

[47] H. Nishimori, *Statistical Physics of Spin Glasses and Information Processing: An Introduction*, International series of monographs on physics (Oxford University Press, 2001).

[48] Rajendra Bhatia, *Matrix analysis*, Vol. 169 (Springer Science & Business Media, 2013).

[49] Bo-Yan Xi and Fuzhen Zhang, "Inequalities for selected eigenvalues of the product of matrices," Proc. Amer. Math. Soc. **147**, 3705–3713 (2019).

[50] F. L. Metz, I. Neri, and T. Rogers, "Spectral theory of sparse non-hermitian random matrices," Journal of Physics A: Mathematical and Theoretical **52**, 434003 (2019).

[51] B. Bravi, M. Opper, and P. Sollich, "Inferring hidden states in langevin dynamics on large networks: Average case performance," Phys. Rev. E **95**, 012122 (2017).

[52] S. F. Edwards and R. C. Jones, "The eigenvalue spectrum of a large symmetric random matrix," Journal of Physics A: Mathematical and General **9**, 1595 (1976).